



OPEN ACCESS

EDITED BY

Guoxin Zhang,
Shandong University of Science and
Technology, China

REVIEWED BY

Min Wang,
Northeastern University, China
Weinan Xing,
Nanjing Forestry University, China
Yingping Huang,
China Three Gorges University, China

*CORRESPONDENCE

Baikang Zhu,
zszbk@zjou.edu.cn
Xianlei Chen,
zschexl@163.com
Hengcong Tao,
hengcongtao@zjou.edu.cn

*These authors have contributed equally
to this work

SPECIALTY SECTION

This article was submitted to
Environmental Nanotechnology,
a section of the journal
Frontiers in Nanotechnology

RECEIVED 19 August 2022

ACCEPTED 05 October 2022

PUBLISHED 19 October 2022

CITATION

Huang J, Li C, Hao H, Li L, Zhu B, Chen X
and Tao H (2022), Photocatalytic
degradation of tetracycline antibiotic
over a flower-like S-doped BiOBr:
Performance, mechanism insight and
toxicity assessment.
Front. Nanotechnol. 4:1023489.
doi: 10.3389/fnano.2022.1023489

COPYRIGHT

© 2022 Huang, Li, Hao, Li, Zhu, Chen
and Tao. This is an open-access article
distributed under the terms of the
[Creative Commons Attribution License
\(CC BY\)](https://creativecommons.org/licenses/by/4.0/). The use, distribution or
reproduction in other forums is
permitted, provided the original
author(s) and the copyright owner(s) are
credited and that the original
publication in this journal is cited, in
accordance with accepted academic
practice. No use, distribution or
reproduction is permitted which does
not comply with these terms.

Photocatalytic degradation of tetracycline antibiotic over a flower-like S-doped BiOBr: Performance, mechanism insight and toxicity assessment

Jianghua Huang^{1†}, Cunjun Li^{2†}, Huadong Hao², Liang Li²,
Baikang Zhu^{1,3*}, Xianlei Chen^{2*} and Hengcong Tao^{1,3,4*}

¹School of Petrochemical Industry and Environment, Zhejiang Ocean University, Zhoushan, Zhejiang, China, ²Zhoushan Institute of Calibration and Testing for Quality and Technology Supervision, Zhoushan, Zhejiang, China, ³United National-Local Engineering Laboratory of Oil & Gas Storage and Transportation, Zhoushan, Zhejiang, China, ⁴College of Chemical and Biological Engineering, Zhejiang University, Hangzhou, China

A new catalyst of S-BiOBr flower-like morphology was synthesized by simple pyrolysis and further used for photocatalytic degradation of TC. Phase structure analysis, elemental analysis and micromorphological analysis confirmed that S doping has a reinforcing effect on the polarization between the $[\text{Bi}_2\text{O}_2\text{S}]^{2+}$ and $[\text{Br}_2]^{2-}$ layers and is conducive to interlayer polarization and rapid charge transfer. In addition, its unique petal morphology is more favorable to the adsorption of contaminants on its surface and accelerates the reaction of catalyst surfactant with contaminants. It was also found that S-BiOBr degrades TC significantly better than single BiOBr@HCs, with up to 99.1% in 60 min illumination. In addition, the S-BiOBr catalyst has good reusability in antibiotic degradation. The results of photocatalytic mechanism analysis show that free radical O_2^- plays a major role in the photodegradation of organic model pollutants. Intermediates in TC degradation were identified, and their potential degradation pathways were prospected, and the toxicity development of TC in the degradation process was analyzed by toxicity assessment software. The S-BiOBr photocatalytic system developed in this paper provides a new idea for effective modification of bismuth-based semiconductors and has important guiding significance for future water purification.

KEYWORDS

S-doped BiOBr, flower-like structure, internal electric field, tetracycline degradation, photocatalytic degradation

Introduction

Water is the essence of all natural resources, but it is also affected by various organic pollutants (Li et al., 2020; Zhang et al., 2020; Wagner et al., 2021). In particular, pharmaceutical and personal care products (PPCPs) have resulted in significant antibiotic discharges, posing a serious threat to the safety of aquatic ecosystems (Wang et al., 2018a) and human health (Rodriguez-Mozaz et al., 2015; Hena et al., 2021). Tetracycline antibiotics and their residues, as pseudo-persistent pollutants, have a wide range of use in drug synthesis, animal feeding, clinical application, and other fields (Scaria et al., 2021; Ahmadijokani et al., 2022; Biswal and Balasubramanian, 2022; Warner et al., 2022). The possible adverse effects on human beings and aquatic ecosystems have become a topic of great concern (Zhu et al., 2013). It is therefore crucial to explore an efficient method for removing tetracycline from the aquatic environment.

Photocatalytic water treatment, powered by renewable solar energy, has attracted increasing attention because of its ability to efficiently degrade antibiotics compared to traditional methods (Chen et al., 2022a; Ha et al., 2022). In addition, the photocatalytic method has many significant advantages, such as high efficiency, clean, pollution-free, etc. (Kang et al., 2019; Sun et al., 2020; Yang et al., 2021; An et al., 2022; Castilla-Caballero et al., 2022). More recently, bismuth-based semiconductors have good prospects with unique light absorption that can enhance photocatalytic activity significantly. Such as Bi_2MoO_6 (Chen et al., 2022b; Hajiali et al., 2022), Bi_2O_3 (Chen et al., 2022c; Entezami et al., 2022), BiVO_4 (Kang et al., 2019; Xu et al., 2021), Bi_2WO_6 (Li et al., 2022a; Li et al., 2022b), BiOBr (Wang et al., 2022a; Dou et al., 2022). As a novel photocatalyst, BiOBr consists of positive $[\text{Bi}_2\text{O}_2]^{2+}$ and negative halogen atoms (Br_2^{2-}) (Lee et al., 2020), while forming unique layered structures (Gao et al., 2022). Such structures allow the insertion of different species into the interlamellar space *via* anion exchange (Li et al., 2015; Wang et al., 2018b; Huang et al., 2020). Some properties, however, such as rapid recombination of photogenerated charge carriers and relatively low light absorption, greatly limit their practical application in environmental protection.

In addition, internal electric field-driven charge separation has become a hot topic in BiOX (Liu et al., 2022a). Its unique layered structure is beneficial for stacking to form built-in electric fields (IEF) (Li et al., 2016), and can facilitate the efficient degradation of pollutants by adding different species exchanges to the laminated space. For example, the IEF tuning of C-doped $\text{Bi}_3\text{O}_4\text{Cl}$ greatly improves the charge transfer efficiency (Li et al., 2014). Bi modification and phosphorylation of BiOBr enhanced its charge separation ability and obtained excellent photocatalytic performance (Zhu et al., 2019). N-doped BiOBr catalysts, were prepared by microwave-assisted solvothermal synthesis, increasing their

specific surface area and photocatalytic activity (López-Velázquez et al., 2021). Therefore, the tuning method of IEF based on non-metal doping is usually beneficial for enhancing interlayer polarization to oxidize organic pollutants.

Owing to their excellent electronic conductivity, stability and electronic storage capacity, carbon materials have been developed as ideal photocatalysts, and the most common type of photocatalyst is the carbon-based material (Sun et al., 2022; Chen et al., 2023). At present, the existing carbon materials mainly include porous nanosheets (Liu et al., 2022b; Liu et al., 2022c), hollow nanotubes (Liu et al., 2022d; Zhang et al., 2022) and three-dimensional (3D) nanospheres (Huang et al., 2021; Serra-Pérez et al., 2021; Wang et al., 2022b), among which, hollow carbon nanospheres (HCs) is one of the ideal carrier materials, due to its fast electron transfer rate, rich active sites, high specific surface area, has been widely studied. So far, template-assisted methods have been used to synthesize microspheres and uniformly deposit other nanoparticles on the surface of HCS to change the semiconductor structure, improve electron conduction efficiency and achieve the goal of pollutant degradation.

In this study, S- BiOBr photocatalyst was synthesized by a simple one-step solvothermal method to degrade tetracycline antibiotics. The addition of glucose to S- BiOBr by the hydrothermal process can change the surface morphology of S- BiOBr , promote the exposure of active sites and polarization of interlayer structures, and effectively prevent the recombination of photogenic electron pore pairs, enhance their photocatalytic activity and efficiently degrade antibiotics.

Experimental details

Chemicals and reagents

Tetracycline ($\text{C}_{22}\text{H}_{24}\text{N}_2\text{O}_8$), Bismuth nitrate pentahydrate ($\text{Bi}(\text{NO}_3)_3 \cdot 5\text{H}_2\text{O}$), Potassium bromide (KBr), D-(+)-Glucose ($\text{C}_6\text{H}_{12}\text{O}_6$), p-Benzoquinone ($\text{C}_6\text{H}_4\text{O}_2$), Sodium dodecyl sulfate ($\text{CH}_3(\text{CH}_2)_{11}\text{OSO}_3\text{Na}$), Ammonium oxalate monohydrate ($(\text{NH}_4)_2\text{C}_2\text{O}_4 \cdot \text{H}_2\text{O}$), Isopropyl Alcohol ($\text{C}_3\text{H}_8\text{O}$), Potassium ferricyanide ($\text{K}_3\text{FeC}_6\text{N}_6$, Sigma Aldrich, 99.5%), Potassium ferrocyanide trihydrate ($\text{K}_4\text{FeC}_6\text{N}_6 \cdot 3\text{H}_2\text{O}$), Potassium chloride (KCl), Sodium sulfate anhydrous (Na_2SO_4), Glycerol ($\text{C}_3\text{H}_8\text{O}_3$), Ethanol ($\text{CH}_3\text{CH}_2\text{OH}$).

Synthesis of photocatalyst

S- BiOBr @HCs was prepared by one-step hydrothermal method. 3 mmol $\text{Bi}(\text{NO}_3)_3 \cdot 5\text{H}_2\text{O}$ was added to 50 ml mixed solution A (glycerol: deionized water = 2:3) and dissolved by ultrasound. 3mmol KBr, 0.432 g glucose and a certain mole of sodium dodecyl sulfate (SDS) were added to 10 ml deionized

water and stirred for 1 h. In constant stirring, drop solution B into solution A at the rate of 1 drop per second, and continue stirring for 0.5 h. Finally, the evenly mixed solution was transferred to a 100 ml Teflon-lined stainless-steel autoclave and heated at 160 °C for 12 h. After cooling at room temperature, wash with deionized water and ethanol for three times and vacuum dry at 60°C for 12 h. SDS of 50, 100, 150, 200 mg, 250 mg, according to different SDS of the amount of added, respectively, SBB-50, SBB-100, SBB-150, SBB-200, SBB-250. BiOBr@HCS are prepared in the same way as above by removing sodium dodecyl sulfate during preparation.

BiOBr@HCS are prepared the same way as above by removing sodium dodecyl sulfate during preparation. In order to obtain various mass ratios of HCS to BiOBr, the total mass of HCS precursor added during the synthesis process caused the mass percentage of as-obtained hybrids to 0, 5, 10, 15, 20 and 30 wt%, which were denoted BiOBr, BiOBr-5, BiOBr-10, BiOBr-15, BiOBr-20 and BiOBr-30.

Characterizations

The Brunauer–Emmett–Teller (BET) surface area was measured using a Micromeritics ASAP 2460. The morphology structure of the synthesized samples were observed with transmission electron microscopy (TEM, JEOL JEM-2100F), and scanning electron microscopy (SEM, ZEISS Sigma 300). Powder X-ray diffraction patterns of the prepared material were recorded on a Dandong Fangyuan X-ray diffractometer copper Cu K α radiation diffraction (Voltage = 40 kV, current = 15 Ma, scanning step = 0.02). Analysis of chemical compositions of the synthesized samples was performed by X-ray spectroscopy of Photoelectrons (XPS, Thermo Scientific ESCALAB Xi+). The UV–vis diffusion-reflectance spectra (UV–vis DRS, Puxi TU-1900) were used to acquire data on light absorption ability. The Mott-Schottky diagrams (MS), transient photocurrent responses (TPR) and electrochemical impedance spectra (EIS) were measured using a CHI660E electrochemical workstation equipped with a three-electrode cell. The Photoluminescence spectra of synthesized samples were collected using an Edinburgh FLS1000 fluorescence spectrophotometer.

Photocatalytic tetracycline degradation experiments

The photocatalytic properties of the synthetic catalyst were evaluated using tetracycline (20 mg L⁻¹, 100 ml) as a model contaminant ($\lambda > 420$ nm) irradiated by a 300 W Xe lamp (Beijing China Education AU Lighting Co., Ltd.). The catalyst is usually dispersed with 30 mg in TC solution. Absorption-desorption equilibrium was established by magnetically stirring the suspension in darkness for 20 min. In this case, the

suspension is exposed to visible light. During the reaction, 2 ml of suspension was collected at predetermined time intervals and filtered through a 0.22-micron membrane. The TC concentration was determined using a UV-Vis spectrophotometer at 357 nm wavelength.

The determination of reactive species

The introduction of different scavengers in the photocatalytic system led to the determination that the main active substances (0.2 mm) in the system of photocatalysis are represented by IPA, BQ, EDTA, etc., the corresponding active radicals being $\cdot\text{OH}$, $\cdot\text{O}_2^-$, or h^+ . The electronic spin resonance (ESR) spectra of DMPO- $\cdot\text{O}_2^-$ were recorded on an electron paramagnetic resonance spectrometer (ESR A300, Bruker).

Detection and evaluation of degradation intermediates

Degradation intermediates were analyzed using the chromatographic column Waters BEH C18 (2.1 \times 100 mm, 1.7 μm) in combination with liquid chromatography-mass spectrometry (Thermo Scientific Q Exactive, United States), with a flow phase of 0.1% formic acid and acetonitrile solution, and a flow rate of 3 ml/min. The temperature of the sheath was set to 350°C, and the flow rate was 12 L/min. The test mode should be set to ESI and the voltage should be set to 4 kV. The detection wavelength for TC was 357 nm. The toxicity of degradation intermediates and TC were appraised by quantitative structure–activity relationship (QSAR) method by using the Toxicity Estimation Software Tool (T.E.S.T. 5.1.1).

Results and discussion

Crystal structure, morphology, and chemical composition

Figure 1 shows the XRD patterns of HCS, BiOBr@HCS and S-BiOBr. It can be shown that the samples were successfully prepared to present good crystallinity. As shown in Figure 1A, The XRD pattern shows that HCS has a broad hump at 22.5°, which indicates an amorphous structure. The diffraction peaks of 10.9°, 25.2°, 31.7°, 32.2°, 46.8° and 57.1° in BiOBr@HCS composite are attributed to the crystal planes of BiOBr (001), (101), (102), (110), (004) and (212) (JCPDS Card No.09-0393), which indicates that the addition of glucose in the synthesis process does not lead to the phase transition of BiOBr nanocrystals. With the increase of glucose content, the characteristic peaks of (001) and (102) crystal planes decreased significantly, indicating that carbon materials affected the characteristic peaks of BiOBr to a

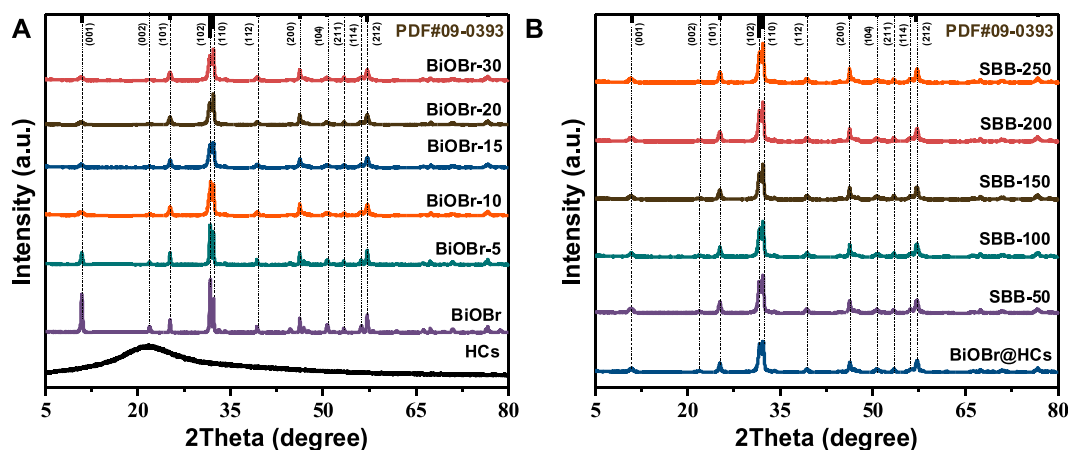


FIGURE 1 XRD pattern of BiOBr@HCs (A) and S-BiOBr (B).

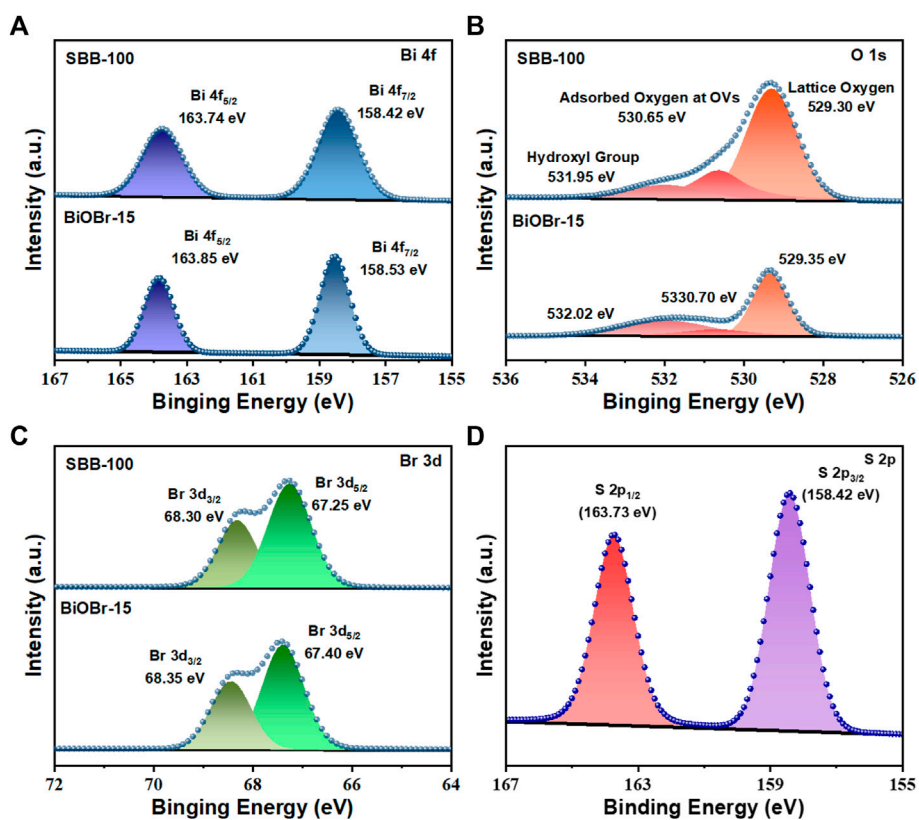


FIGURE 2 (A) Bi 4f, (B) O 1s, (C) Br 3d days XPS spectra of BiOBr-15 and SBB-100, (D) S 2p of SBB-100.

certain extent. Its diffraction peak of the S-BiOBr is consistent with the diffraction peak of BiOBr@HCs and has no miscellaneous peaks, demonstrating that the S-doped BiOBr

structure has good stability (Figure 1B). In addition, with the doping of the S element, the characteristic peak of the (001) phase tends to move to a low Angle direction slightly, and the

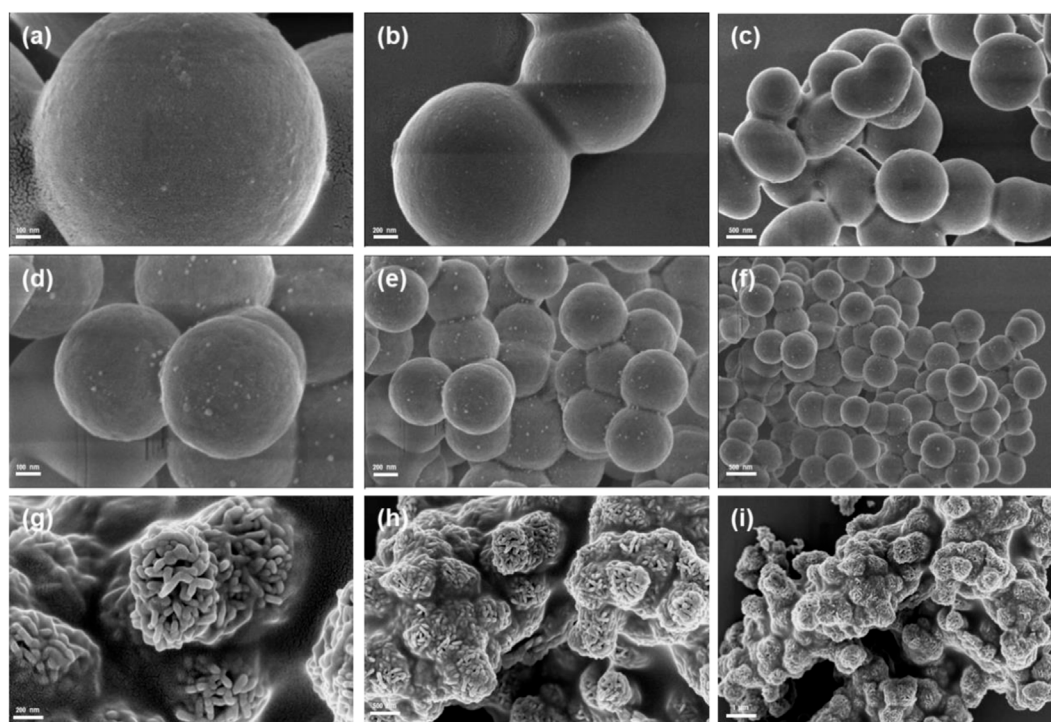


FIGURE 3
Scanning electron microscopy (SEM) images of (A–C) HCs, (D–F) BiOBr-15 and (G–I) SBB-100.

characteristic peak of the (110) phase gradually increases (Supplementary Figure S1). This may indicate that the doping of the S element extends the interlayer space of the composite and improves the charge separation efficiency of the built-in electric field.

In order to confirm additional evidence of S doping, bonding interactions and chemical states of BiOBr-15 and SBB-100 were characterized by XPS spectroscopy (Figures 2A–D). As shown in Figure 2A, the binding energy is located at 163.74 and 158.42 eV corresponding to Bi 4f_{5/2} and Bi 4f_{7/2} (Jiang et al., 2021; Meng et al., 2021). The position of Br 3d peaks was adjusted from 68.35 to 67.40 eV to 67.30 and 67.25 eV, respectively, due to the addition of the S element, which resulted in a weakening of the interaction between the positional and negative electron layers of BiOBr, and the partial replacement of Br⁻ by S²⁻ (Figure 2B). Compared with BiOBr-15, SBB-100, which has the same binding energy form, is transferred to a lower energy direction, possibly because of the noticeable electronic shift of S to Bi through Bi-S bond, thus forming the interaction interface. Figure 2C shows the spectrum of O 1s, with 529.30, 530.65 and 531.95 eV representing lattice oxygen, adsorbed vacancy oxygen and surface hydroxyl group (Zhou et al., 2020). Compared with BiOBr-15, the peak of lattice oxygen was reduced by 0.05 eV, along with a significant increase in the oxygen adsorbed at the vacancies (OVs), which indicates that more oxygen vacancies are exposed on the surface

of the material. The adsorption effect of catalyst on O₂ molecule was enhanced after the addition of S element. The diffraction peaks at 163.73 and 158.42 eV in S 2p are attributed to S 2p_{1/2} and S 2p_{3/2}, respectively, which also confirm the successful doping of S elements in SBB-15 (Figure 2D). Consequently, the above results indicate that the addition of the S element is associated with the [Bi₂O₂]²⁺ active electron layer, resulting in the ideal [Bi₂O₂S]²⁺ layer that produces rich OV.

The morphology and structure of the prepared catalysts were observed by SEM. Figures 3A–C showed the SEM image of HCs. Hollow carbon spheres (HCs) form uniform spheroids with a diameter of about 1.2 μm, which is consistent with the description in the literature (Du et al., 2022). After adding glucose in BiOBr preparation, the BiOBr nanoparticles were deposited on the surface of the carbon sphere during the hydrothermal process, and the overall diameter was changed from 1.2 μm to 0.5 μm (Figures 3D–F). After the addition of the S element in the hydrothermal process, the overall morphology of the catalyst changed, possibly because the doping of the S source in the preparation process caused the ring-opening reactions of glucose, which made the successfully prepared SBB-100 transform into the shape of nanorods (Figures 3G–I).

TEM and high resolution TEM (HRTEM) were employed. As shown in Figures 4A,B, plenty of SBB-100 nanorods (size~100 nm) were tightly agglomerated and formed 3D

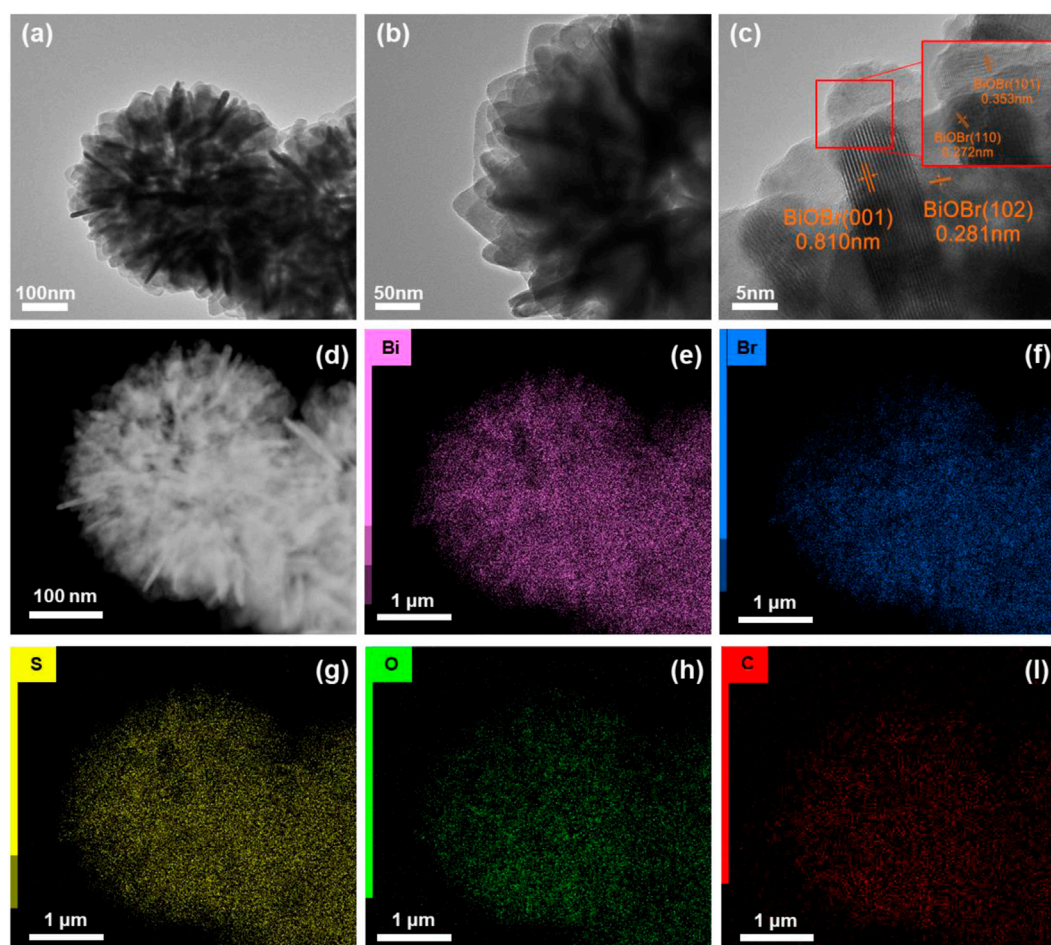


FIGURE 4
 (A, B) Transmission electron microscopy (TEM) images, (C) high-resolution TEM (HRTEM) images and (D–I) elemental mapping of SBB-15.

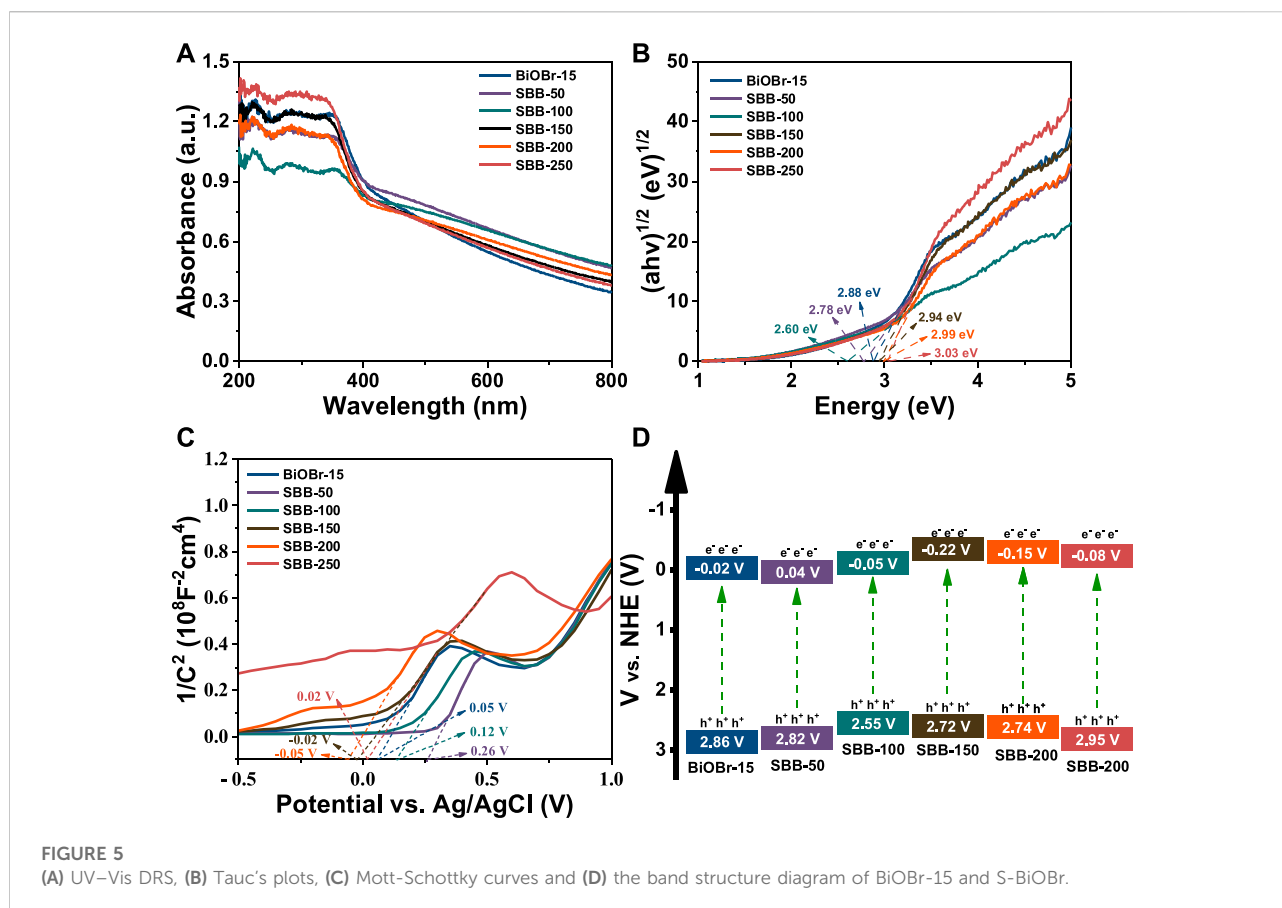
flower-like structures, consistent with SEM characterization. Remarkably, the interlayer distance became larger as element S was introduced, contributing to the ultrathin nanorods. Further examination of the crystalline of SBB-15 was performed by collecting the HRTEM image and showing it in Figure 4C. Four crystal surfaces, 0.810, 0.353, 0.281, and 0.272 nm, were observed in the figure, belonging to (001), (1001), (102), and (1100) crystal surfaces of BiOBr, respectively. In addition, EDS-mapping spectra indicate the distribution of elements Bi, Br, S, O and C in SBB-100. This is evidence of the successful construction of S-BiOBr, a structure that will facilitate effective charge separation.

The hierarchical structure of BiOBr@HCs was intercalated with S-element to obtain its petal-like morphology. The BET test results are shown in Supplementary Figure S2. HCAs, BiOBr-15 and SBB-100 all exhibit Class IV isotherms, the surface area and pore diameter distributions of the samples are presented in Supplementary Table S1. Notably, SBB-100 possesses a higher

BET surface area ($26.89 \text{ m}^2 \text{ g}^{-1}$) than pristine BiOBr-15 ($20.26 \text{ m}^2 \text{ g}^{-1}$) and HCAs ($5.13 \text{ m}^2 \text{ g}^{-1}$). It is expected to provide additional reactant exposure sites and increase electron charge transfer pathways.

Characterization of optical properties

Optical characteristics of BiOBr-15 and S-BiOBr were characterized by UV-Vis (Figure 5A). Both BiOBr-15 and S-BiOBr exhibit intense visible-light absorption. With the increase of S doping content, the absorption boundary shifts to the visible light region. SBB-100 improves the absorption of visible light, and the introduction of S broadens the photo-absorption range of BiOBr, contributing to its photocatalytic behavior. The E_g values of BiOBr-15 (2.88 eV) and S-BiOBr, (2.78, 2.60, 2.94, 2.99, and 3.03 eV) were calculated by Kubelka-Munk formula (Figure 5B).



In addition, the Mott-Schottky test revealed that both BiOBr-15 and S-BiOBr present n-type semiconductor characteristics (Figure 5C) (Liu et al., 2022e; Yin et al., 2022). Moreover, the flat band potential (E_{fb}) could be obtained by extrapolating the tangent line of the x-axis intercept. The E_{fb} of BiOBr-15 and S-BiOBr is determined to be 0.12, 0.26, 0.05, -0.02, -0.05 and 0.02 V (vs. Ag/AgCl). Furthermore, the E_{CB} of n-type semiconductor is about 0.1 V higher than that of E_{fb} , so the E_{CB} of BiOBr-15 and S-BiOBr are about -0.22, -0.16, -0.25, -0.32, -0.35 and -0.28 V (vs. Ag/AgCl). According to Eq. 1, their corresponding E_{NHE} were obtained as -0.02, 0.04, -0.05, -0.22, -0.15 and -0.08 V (vs. the normal hydrogen electrode, NHE), respectively.

$$E_{NHE} = E_{Ag/AgCl} + 0.197. \quad (1)$$

Hence, the E_{VB} of BiOBr-15 and S-BiOBr are calculated as 2.86, 2.82, 2.55, 2.72, 2.74 and 2.95 V (vs. NHE), respectively, using the Nernst formula:

$$E_{CB} = E_{VB} - E_g. \quad (2)$$

The band structures of BiOBr-15 and S-BiOBr are shown in Figure 5D.

Photocatalytic activity

Photocatalytic activity of visible light irradiating photocatalyst (Figures 6A,B) was determined using TC as contaminant. Supplementary Figure S3 shows the TC degradation efficiency of BiOBr@HCs. It can be clearly observed that BiOBr-15 has the highest degradation efficiency, which can reach 76.3%, which is significantly improved compared with pure BiOBr (59.4%). As shown in Figure 6A, after irradiation for 120 min, the TC degradation efficiency of BiOBr-15 was only 59.4% respectively, because of the severe recombination of photogenerated carriers. Interestingly, with the increase of S element, the resulting S-BiOBr had remarkably enhanced photocatalytic degradation efficiency. Among them, SBB-100 exhibited the best degradation effect, which can reach 99.1% after 60 min of irradiation (Figure 6A). However, with increasing S content, the photocatalytic activity decreases, possibly because of the excessive doping of S elements leading to the destruction of BiOBr-15 and the decrease of charge separation efficiency. Further, the adsorption properties of BiOBr-15 and S-BiOBr are almost negligible. When the ratio of S to BiOBr-15 reached the optimal value (SBB-100), the adsorption performance gradually

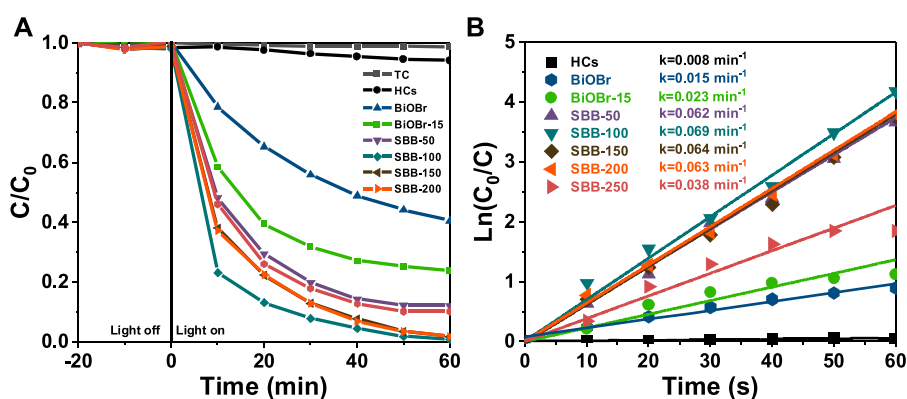


FIGURE 6 (A) Degradation curves and (B) the pseudo-first-order kinetics of HCs, BiOBr@HCs and S-BiOBr (30 mg) for tetracycline (TC) (20 mg/L, 100 ml).

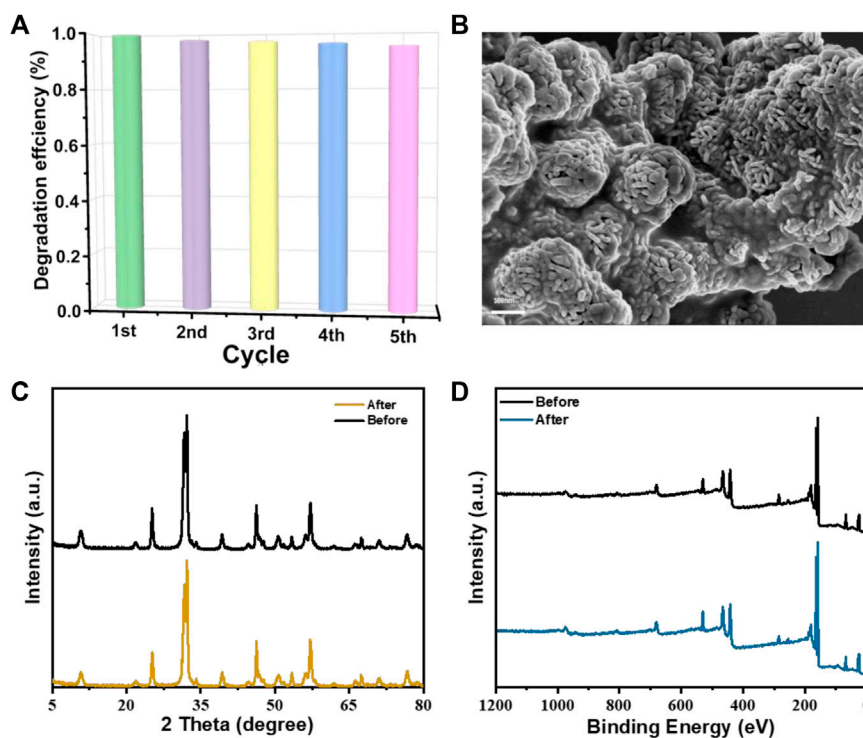


FIGURE 7 (A) Recycling performance of SBB-100 for TC degradation, (B) SEM image of used SBB-100, (C) XRD and (D) XPS of the fresh and used SBB-100.

decreased, proving that SBB-100 has the largest specific surface area and the smallest average pore size among all the catalysts. Among these materials, SBB-100 has the best adsorption capacity and the highest photocatalytic activity. The results show that the morphology of SBB-100 makes it have more active sites, and the built-in electric field constructed by SBB-100 can better separate photogenerated electron-hole pairs. In addition, the degradation

conforms to the pseudo-first-order kinetics: $\ln(C_0/C) = kt$ (4). The degradation curves are shown in Figure 6B. SBB-100 has the highest degradation k value of 0.069 min^{-1} for TC, which is 2.68 folds higher than that of BiOBr (0.023 min^{-1}).

The stability of practical application is also an important factor of the ideal photocatalyst. Therefore, the stability of SBB-100 was evaluated by cyclic assays (Figure 7). SBB-100 showed no

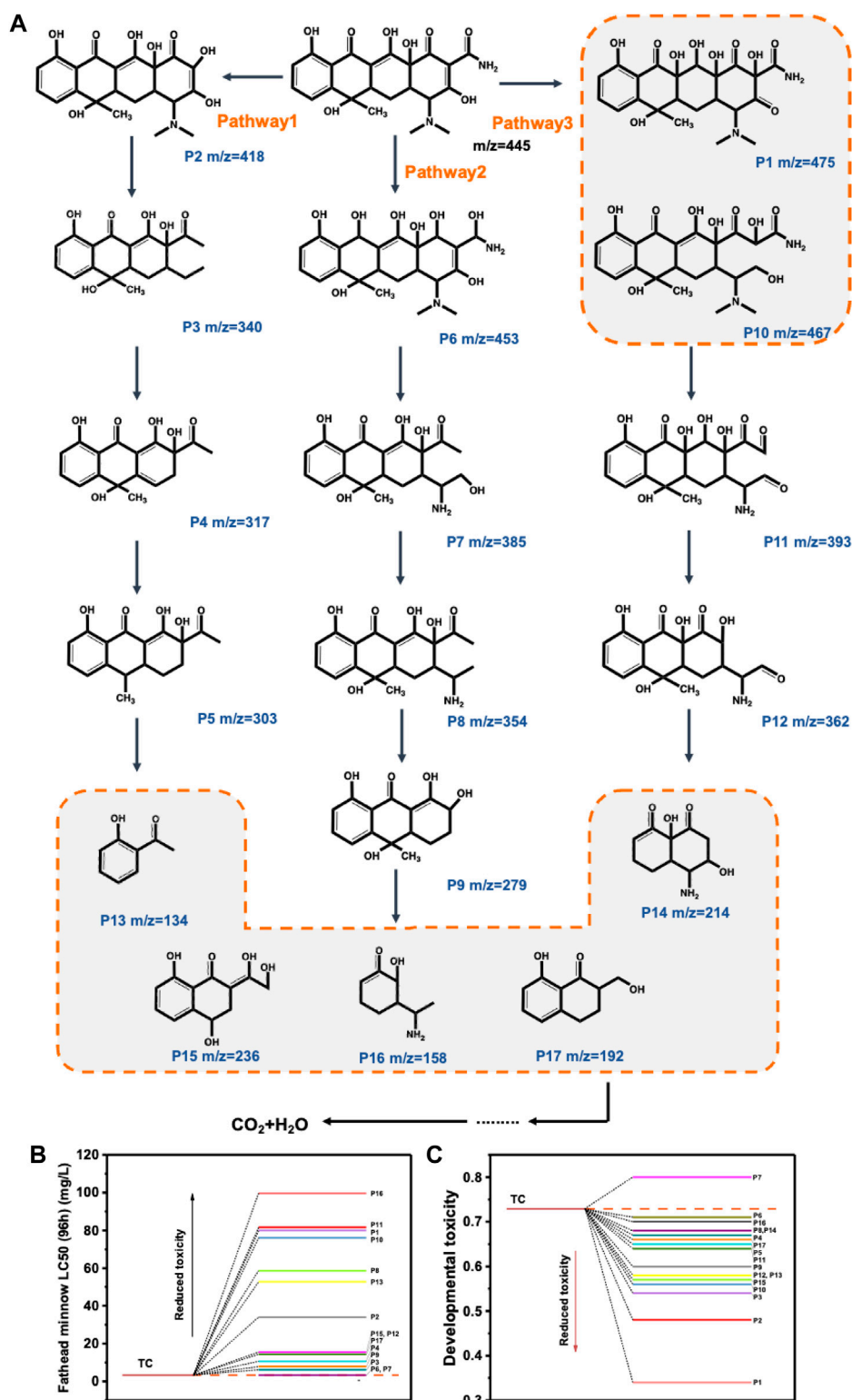


FIGURE 8 The possible TC photocatalytic degradation pathways over SBB-100 (A); Evaluation of TC and its degradation intermediates for acute (B) and developmental toxicity (C).

significant inactivation and TC degradation remained at 94.9% after five consecutive cycles (Figure 7A). In addition, the SEM image, XRD pattern and XPS spectrum further showed that the morphology and properties of the catalyst did not change during the photocatalysis. The results show that SBB-100 owns the advantages of high activity, mineralization ability, stability, and reusability, and has broad application prospects in practical wastewater treatment.

Possible degradation pathways and toxicity assessment of intermediates

SBB-100-induced tetracycline degradation was investigated by HPLC-MS (Supplementary Figure S31, Supplementary Table S2). In this paper, three main degradation pathways of tetracycline by SBB-100 to tetracycline were proposed. For Pathway 1, the original tetracycline was gradually demethylated to P2 by photoinduced superoxide radical invasion, followed by further conversion to P3 by O_2^- and h^+ induced open-loop reactions. Demethylation produces P4 when P3 is attacked by highly reactive OH and h^+ , and P4 is further converted to P5 when hydroxyl is lost. For Pathway 2, tetracycline is first converted to P6 by carbonyl reduction, then formed into P7 by C = C rupture, followed by a dehydroxy reaction at h^+ , $\cdot O_2^-$ co-action to produce P8. The formation of P9 was attributed to aldehyde loss, deammonia and demethylation. For Pathway 3, the hydroxylation reaction happens to produce P1 because C = C double bond is extremely unstable and prone to oxidation. In addition, P10 was formed by an open-loop reaction induced by O_2^- and h^+ . The strong ionization of O_2^- causes P1 to break the C-C bond and further transform into P11. At the same time, P10 can be further transformed into P11 by the loss of amide groups to form ketogenic groups. Secondly, the formation of P12 is due to the elimination of formaldehyde. In addition, intermediates of these pathways were converted to P13, P14, P15, P16 and P17. Eventually, these intermediates are broken down into small molecules and mineralized under the action of active substances.

The degradation products were evaluated for acute toxicity and developmental toxicity using Toxicity Estimation Software (TEST 5.1.1). As shown in Figure 8B represents the dose at which half of the fathead minnow was killed in 96 h, an important parameter for measuring the toxicity of the product in the aquatic environment. Therefore, the lethal concentration of TC was up to 3.33 mg/L, and most of the intermediate products were lower than that of TC except for P6 and P7. Furthermore, as can be observed in Figure 8C, the developmental toxicity of the TC intermediates produced during photodegradation [except P7 (0.8)] is correspondingly reduced. The results show that S-BiOBr is effective as a photocatalyst in reducing or mitigating the threat to human health posed by various pollutants in the environment.

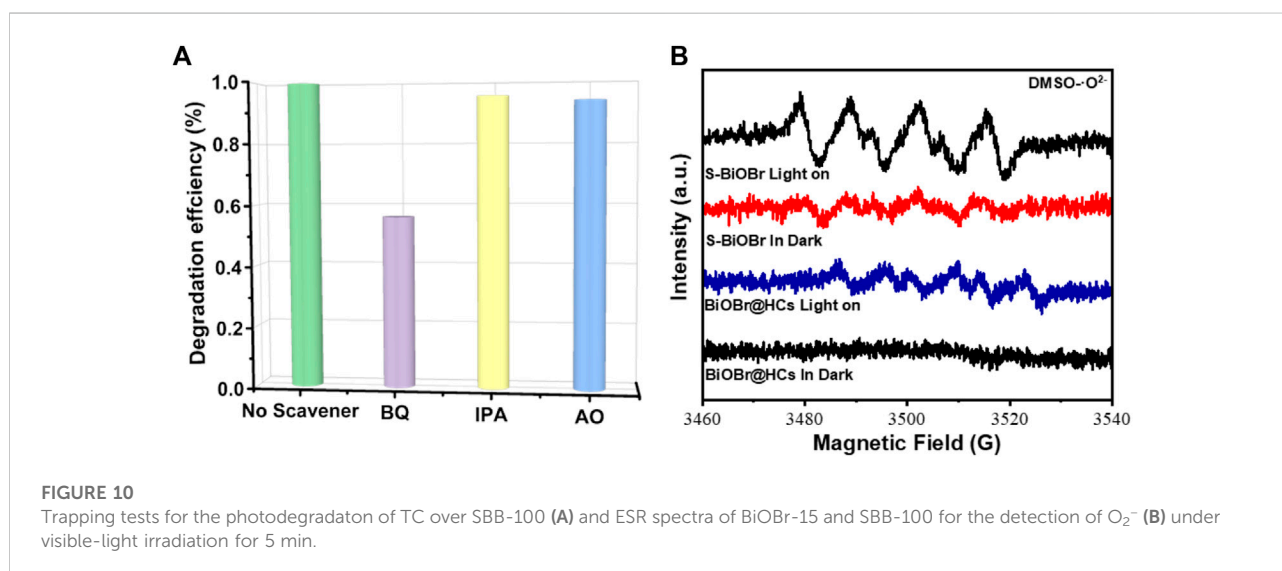
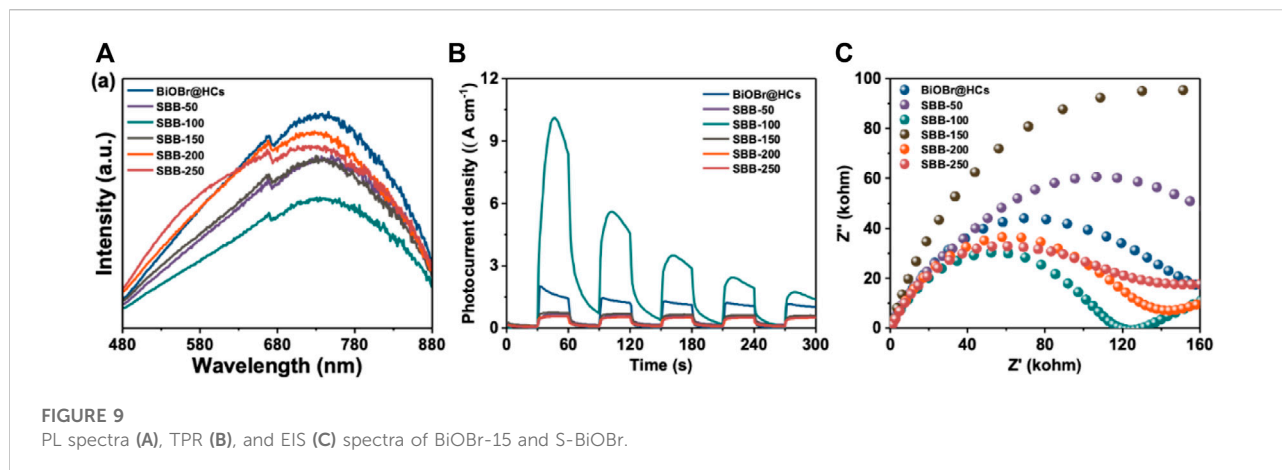
Photocatalytic degradation mechanism

In order to elucidate further the enhanced photocatalytic properties of BiOBr-15 and S-BiOBr, a series of characterizations including PL, TPR, and EIS were carried out to investigate photo generated carrier separation behavior in as-fabricated samples (Figure 9). PL spectra of BiOBr-15 and S-BiOBr [the excitation wavelength (λ_{ex}): 735 nm] are shown in Figure 9A. In general, the higher the characteristic peak intensity of the photoluminescence spectrum, the easier it is for the carrier to recombine. S-BiOBr showed a lower peak area compared to BiOBr-15, reflecting that S-BiOBr construction did hinder electron pore recombination. It is beneficial to increase the charge transfer of the catalyst interface, especially the energy transfer of S-BiOBr interlayer electric field, and thus the photocatalytic performance of S-BiOBr. Of these, SBB-100 had the lowest PL intensity, suggesting that SBB-100 has more carrier transport for pollutant decomposition.

In addition, the generation and separation of photogenic carriers are studied in detail by using the transient photoreactive current spectra under visible light to better understand the transfer and separation of photogenic carriers. It is evident from Figure 9B that S-BiOBr exhibits excellent optical response under visible illumination during the interval between 30 s as light source switches. And during this process, the material is stable to the current generated by visible light. SBB-100 exhibited the highest photocurrent response of all catalysts, which exhibited high separation efficiency and long carrier life.

Furthermore, the transfer characteristics of carriers were investigated by measuring the electrochemical impedance spectra of photocatalysts. As can be seen from Figure 9C, SBB-100 corresponds to the smallest graph radius, representing a minimum charge transfer resistance. It can be explained that SBB-100 can transfer charges more easily on its interface and effectively separate photon carriers. The above experimental results show that SBB-100 polarizes its interlayer electric field, greatly improves the generation and transfer of interface charges, and improves the performance of photocatalytic degradation.

Reactive oxygen species (ROS) play a major role in photocatalytic degradation experiments, the trapping experiments as well as ESR analyses were carried out. Results of the trapping experiments are shown in Figure 10A. In the absence of scavenging agent, 99.1% of TC can be observed to be degraded by SBB-100. It is clear from trapping experiments that the TC degradation efficiency decreased from 99.1% to 56.1% with the addition of P-benzoquinone, which indicates that $\bullet O_2^-$ is the predominant reactive species accounting for TC degradation. As shown in Figure 10B, DMPO- O_2^- signal was detected after 5 min of visible light irradiation. Interestingly, the intensity of the DMPO- O_2^- signal produced on SBB-100 was remarkably stronger than that of the original BiOBr-15,



suggesting that more O_2^- free radicals were produced in the S-BiOBr system.

Based on the above analysis, the main reasons for upgrading S-BiOBr photocatalytic activity are as follows. In this study, S-BiOBr increased the specific surface area, and antibiotics were effectively adsorbed and in close contact with the interface. The addition of the S element changes the interlayer structure of the BiOBr, forming two layers $[Bi_2O_2S]^{2+}$ and $[Br_2]^{2-}$, whose unique layered structure stacks to create the built-in electric field. The UV-Vis and Mott-Schottky curves show that the band structure of SBB-100 is shortened. S doping enhances the polarization between $[Bi_2O_2S]^{2+}$ and $[Br_2]^{2-}$ layers, promotes the exposure of the active site, and significantly improves the separation and migration efficiency of photogenerated

electron-hole pairs. Moreover, XPS and PL test results show that SBB-100 produces more oxygen vacancies, leading to an upward shift in the Fermi level (E_f). Dissociation of excitons promotes the generation of charge carriers, resulting in the production of more superoxide radicals, consistent with ESR test results. In the degradation process, superoxide radicals transfer to the contact interface between TC and SBB-100 to degrade the TC adsorbed on the surface. In addition, PL, TPR and EIS experiments also show that SBB-100 has the advantages of the highest separation efficiency of photogenerated electron-hole pairs, the largest instantaneous photocurrent in the visible light range, and the fastest electron migration efficiency, which makes it one of the best materials in the same category.

Conclusion

A novel S-doped BiOBr photocatalyst was triumphantly synthesized by the isothermal method. S-BiOBr has a substantial photocatalytic effect on TC antibiotics under visible light. The unique layered structure of S-BiOBr is composed of $[\text{Bi}_2\text{O}_2\text{S}]^{2+}$ and $[\text{Br}_2]^{2-}$ and exhibits highly efficient photocatalytic degradation of tetracycline. HPLC-MS analysis was used to demonstrate the possible degradation pathways. The toxicity of the degradation intermediates was evaluated by Toxicity Estimation Software (TEST 5.1.1). It showed that TC in the S-BiOBr system not only achieved businesslike degradation, but also remarkably reduced toxicity. Eventually, the photocatalytic mechanism of S-BiOBr is proposed on the basis of the reaction state capture experiment and ESR analysis. Accordingly, we respect that this work not only proposes a feasible path in order to gain single-atom doped materials for the degradation of pharmaceutical antibiotics, but also has enlightening significance for future exploration of environmental restoration.

Data availability statement

The original contributions presented in the study are included in the article/Supplementary Material, further inquiries can be directed to the corresponding authors.

Author contributions

All authors listed have made a substantial, direct, and intellectual contribution to the work and approved it for publication.

References

- Ahmadijokani, F., Molavi, H., Tajahmadi, S., Rezakazemi, M., Amini, M., Kamkar, M., et al. (2022). Coordination chemistry of metal-organic frameworks: Detection, adsorption, and photodegradation of tetracycline antibiotics and beyond. *Coord. Chem. Rev.* 464, 214562. doi:10.1016/j.ccr.2022.214562
- An, W., Hu, S., Yang, T., Wang, H., Hu, J., Cui, W., et al. (2022). Oxygen vacancies enhance Fe-doped BiOCl photocatalysis-Fenton synergy degradation of phenol. *Mater. Lett.* 322, 132466. doi:10.1016/j.matlet.2022.132466
- Biswal, B. K., and Balasubramanian, R. (2022). Adsorptive removal of sulfonamides, tetracyclines and quinolones from wastewater and water using carbon-based materials: Recent developments and future directions. *J. Clean. Prod.* 349, 131421. doi:10.1016/j.jclepro.2022.131421
- Castilla-Caballero, D., Sadak, O., Martínez-Díaz, J., Martínez-Castro, V., Colina-Márquez, J., Machuca-Martínez, F., et al. (2022). Solid-state photocatalysis for plastics abatement: A review. *Mater. Sci. Semicond. Process.* 149, 106890. doi:10.1016/j.mssp.2022.106890
- Chen, L., Li, Y., Zhang, J., Li, M., Yin, W., and Chen, X. (2022). Oxidative degradation of tetracycline hydrochloride by $\text{Mn}_2\text{O}_3/\text{Bi}_2\text{O}_3$ photocatalysis activated peroxymonosulfate. *Inorg. Chem. Commun.* 140, 109414. doi:10.1016/j.inoche.2022.109414
- Chen, R., Dou, X., Xia, J., Chen, Y., and Shi, H. (2022). Boosting peroxymonosulfate activation over $\text{Bi}_2\text{MoO}_6/\text{CuWO}_4$ to rapidly degrade tetracycline: Intermediates and mechanism. *Sep. Purif. Technol.* 296, 121345. doi:10.1016/j.seppur.2022.121345
- Chen, W., Huang, J., Shen, Y., Zhu, K., Lei, L., He, H., et al. (2023). Fe-N co-doped coral-like hollow carbon shell toward boosting peroxymonosulfate activation for efficient degradation of tetracycline: Singlet oxygen-dominated non-radical pathway. *J. Environ. Sci.* 126, 470–482. doi:10.1016/j.jes.2022.03.018
- Chen, X., Liu, X., Zhu, L., Tao, X., and Wang, X. (2022). One-step fabrication of novel MIL-53(Fe, Al) for synergistic adsorption-photocatalytic degradation of tetracycline. *Chemosphere* 291, 133032. doi:10.1016/j.chemosphere.2021.133032
- Dou, X., Chen, Y., and Shi, H. (2022). $\text{CuBi}_2\text{O}_4/\text{BiOBr}$ composites promoted PMS activation for the degradation of tetracycline: S-Scheme mechanism boosted $\text{Cu}^{2+}/\text{Cu}^+$ cycle. *Chem. Eng. J.* 431, 134054. doi:10.1016/j.cej.2021.134054
- Du, C., Feng, W., Nie, S., Su, X., Liu, H., Feng, J., et al. (2022). π - π conjugation driving degradation of aromatic compounds with *in-situ* hydrogen peroxide generation over $\text{Zn}_2\text{In}_2\text{S}_5$ grown on nitrogen-doped carbon spheres. *Appl. Catal. B Environ.* 310, 121298. doi:10.1016/j.apcatb.2022.121298
- Entezami, N., Farhadian, M., Nazar, A. R. S., and Tangestaninejad, S. (2022). Synthesis and characterization of $\text{Bi}_2\text{O}_3/\text{ZIF-67}$ nanocomposite integration with capacitive deionization system in the degradation tetracycline. *Process Saf. Environ. Prot.* 164, 747–760. doi:10.1016/j.psep.2022.06.059
- Gao, C., Zhang, K., Yi, L., Wang, K., Wu, X., Li, J., et al. (2022). Self-assembled ultrathin closely bonded 2D/2D heterojunction for enhanced visible-light-induced photocatalytic oxidation and reaction mechanism insights. *J. Colloid Interface Sci.* 608, 2472–2481. doi:10.1016/j.jcis.2021.10.173
- Ha, G. H., Mohan, H., Oh, H. S., Kim, G., Seralathan, K.-K., and Shin, T. (2022). Photocatalytic degradation of tetracycline using hybrid $\text{Ag}/\text{Ag}_2\text{S}@/\text{BiOI}$ nanowires:

Funding

NSFC-Zhejiang Joint Fund for Integration of Industrialization and Diversification (U1809214), National Natural Science Foundation of China (No.22005269), Natural Science Foundation of Zhejiang Province (No. LQ21B030007)

Conflict of interest

The authors declare that the research was conducted in the absence of any commercial or financial relationships that could be construed as a potential conflict of interest.

Publisher's note

All claims expressed in this article are solely those of the authors and do not necessarily represent those of their affiliated organizations, or those of the publisher, the editors and the reviewers. Any product that may be evaluated in this article, or claim that may be made by its manufacturer, is not guaranteed or endorsed by the publisher.

Supplementary material

The Supplementary Material for this article can be found online at: <https://www.frontiersin.org/articles/10.3389/fnano.2022.1023489/full#supplementary-material>

- Degradation mechanism and toxicity evaluation. *Chemosphere* 303, 135091. doi:10.1016/j.chemosphere.2022.135091
- Hajiali, M., Farhadian, M., and Tangestaninejad, S. (2022). Novel ZnO nanorods/Bi₂MoO₆/MIL-101(Fe) heterostructure immobilized on FTO with boosting photocatalytic activity for tetracycline degradation: Reaction mechanism and toxicity assessment. *Applied Surface Science*.602, 154389 doi:10.1016/j.apsusc.2022.154389
- Hena, S., Gutierrez, L., and Croué, J.-P. (2021). Removal of pharmaceutical and personal care products (PPCPs) from wastewater using microalgae: A review. *J. Hazard. Mater.* 403, 124041. doi:10.1016/j.jhazmat.2020.124041
- Huang, S., Wang, G., Liu, J., Du, C., and Su, Y. (2020). A novel CuBi₂O₄/BiOBr direct Z-scheme photocatalyst for efficient antibiotics removal: Synergy of adsorption and photocatalysis on degradation kinetics and mechanism insight. *ChemCatChem* 12, 4431–4445. doi:10.1002/cctc.202000634
- Huang, Y., Li, J., Du, P., and Lu, X. (2021). Rational design of copper encapsulated within nitrogen-doped carbon core-shell nanosphere for efficiently photocatalytic peroxymonosulfate activation. *J. Colloid Interface Sci.* 597, 206–214. doi:10.1016/j.jcis.2021.04.016
- Jiang, L., Xie, Y., He, F., Ling, Y., Zhao, J., Ye, H., et al. (2021). Facile synthesis of GO as middle carrier modified flower-like BiOBr and C₃N₄ nanosheets for simultaneous treatment of chromium(VI) and tetracycline. *Chin. Chem. Lett.* 32, 2187–2191. doi:10.1016/j.ccl.2020.12.010
- Kang, N., Xu, D., and Shi, W. (2019). Synthesis plasmonic Bi/BiVO₄ photocatalysts with enhanced photocatalytic activity for degradation of tetracycline (TC). *Chin. J. Chem. Eng.* 27, 3053–3059. doi:10.1016/j.cjche.2019.05.008
- Lee, G.-Y., Cho, E.-C., Lo, P.-Y., Zheng, J.-H., Huang, J.-H., Chen, Y.-L., et al. (2020). Simultaneous formation of Bi₂O₂(OH)(NO₃)/BiOBr ultrathin hierarchical microspheres for effectively promoting visible-light-driven photocatalytic activity in environmental remediation. *Chemosphere* 258, 127384. doi:10.1016/j.chemosphere.2020.127384
- Li, H., Shang, J., Ai, Z., and Zhang, L. (2015). Efficient visible light nitrogen fixation with BiOBr nanosheets of oxygen vacancies on the exposed {001} facets. *J. Am. Chem. Soc.* 137, 6393–6399. doi:10.1021/jacs.5b03105
- Li, J., Cai, L., Shang, J., Yu, Y., and Zhang, L. (2016). Giant enhancement of internal electric field boosting bulk charge separation for photocatalysis. *Adv. Mat.* 28, 4059–4064. doi:10.1002/adma.201600301
- Li, J., Zhang, L., Li, Y., and Yu, Y. (2014). Synthesis and internal electric field dependent photoreactivity of Bi₃O₄Cl single-crystalline nanosheets with high {001} facet exposure percentages. *Nanoscale* 6, 167–171. doi:10.1039/c3nr05246j
- Li, T., He, Y., and Peng, X. (2020). Efficient removal of tetrabromobisphenol A (TBBPA) using sewage sludge-derived biochar: Adsorptive effect and mechanism. *Chemosphere* 251, 126370. doi:10.1016/j.chemosphere.2020.126370
- Li, X., Zhang, H., Du, X., Wang, S., Zhang, Q., Li, H., et al. (2022). Efficient visible-light-driven degradation of tetracycline by a 2D/2D rGO-Bi₂WO₆ heterostructure. *Environ. Res.* 212, 113326. doi:10.1016/j.envres.2022.113326
- Li, Z., Chen, S., Li, Z., Sun, J., Yang, J., Wei, J., et al. (2022). Visible light driven antibiotics degradation using S-scheme Bi₂WO₆/CoIn₂S₄ heterojunction: Mechanism, degradation pathways and toxicity assessment. *Chemosphere* 303, 135113. doi:10.1016/j.chemosphere.2022.135113
- Liu, C., Mao, S., Shi, M., Hong, X., Wang, D., Wang, F., et al. (2022). Enhanced photocatalytic degradation performance of BiVO₄/BiOBr through combining Fermi level alteration and oxygen defect engineering. *Chem. Eng. J.* 449, 137757. doi:10.1016/j.cej.2022.137757
- Liu, J., Liang, H., Li, C., and Bai, J. (2022). Construction of V-doped graphitic carbon nitride with nanotube structure for sustainable photodegradation of tetracycline. *Vacuum* 204, 111342. doi:10.1016/j.vacuum.2022.111342
- Liu, K., Zhang, H., Fu, T., Wang, L., Tang, R., Tong, Z., et al. (2022). Construction of BiOBr/Ti₃C₂/exfoliated montmorillonite Schottky junction: New insights into exfoliated montmorillonite for inducing MXene oxygen functionalization and enhancing photocatalytic activity. *Chem. Eng. J.* 438, 135609. doi:10.1016/j.cej.2022.135609
- Liu, L., Yu, M., Li, Y., Han, C., Ding, G., Liu, S., et al. (2022). Microwave (MW)-assisted design of cobalt anchored 2D graphene-like carbon nanosheets (Co@GCNs) as peroxymonosulfate activator for tetracycline degradation and insight into the catalytic mechanism. *Sep. Purif. Technol.* 295, 121358. doi:10.1016/j.seppur.2022.121358
- Liu, X., Yang, Z., Yang, Y., and Li, H. (2022). Construction of carbon quantum dots sensitized porous carbon nitride/titanium dioxide nanosheets for enhancing visible light photocatalytic degradation of tetracycline. *J. Environ. Chem. Eng.* 10, 108083. doi:10.1016/j.jece.2022.108083
- López-Velázquez, K., Guzmán-Mar, J. L., Montalvo-Herrera, T. J., Mendiola-Alvarez, S. Y., and Villanueva-Rodríguez, M. (2021). Efficient photocatalytic removal of four endocrine-disrupting compounds using N-doped BiOBr catalyst under UV-Vis radiation. *J. Environ. Chem. Eng.* 9, 106185. doi:10.1016/j.jece.2021.106185
- Meng, L., Qu, Y., and Jing, L. (2021). Recent advances in BiOBr-based photocatalysts for environmental remediation. *Chin. Chem. Lett.* 32, 3265–3276. doi:10.1016/j.ccl.2021.03.083
- Rodríguez-Mozaz, S., Chamorro, S., Martí, E., Huerta, B., Gros, M., Sánchez-Melsió, A., et al. (2015). Occurrence of antibiotics and antibiotic resistance genes in hospital and urban wastewaters and their impact on the receiving river. *Water Res.* 69, 234–242. doi:10.1016/j.watres.2014.11.021
- Scaria, J., Anupama, K. V., and Nidheesh, P. V. (2021). Tetracyclines in the environment: An overview on the occurrence, fate, toxicity, detection, removal methods, and sludge management. *Sci. Total Environ.* 771, 145291. doi:10.1016/j.scitotenv.2021.145291
- Serra-Pérez, E., Álvarez-Torrellas, S., Ismael Águeda, V., Larriba, M., Ovejero, G., and García, J. (2021). Effective removal of naproxen from aqueous solutions by CWAO process using noble metals supported on carbon nanospheres catalysts. *Sep. Purif. Technol.* 259, 118084. doi:10.1016/j.seppur.2020.118084
- Sun, H., Xiao, Z., Zhao, Z., Huang, Y., Zhai, S., and An, Q. (2022). Facile synthesis of CaWO₄ nanoparticles incorporated on porous carbons with improved photocatalytic degradation of tetracycline. *Colloids Surfaces A Physicochem. Eng. Aspects* 651, 129790. doi:10.1016/j.colsurfa.2022.129790
- Sun, Y., Qi, X., Li, R., Xie, Y., Tang, Q., and Ren, B. (2020). Hydrothermal synthesis of 2D/2D BiOCl/g-C₃N₄ Z-scheme: For TC degradation and antimicrobial activity evaluation. *Opt. Mater.* 108, 110170. doi:10.1016/j.optmat.2020.110170
- Wagner, M., Andrew Lin, K.-Y., Oh, W.-D., and Lisak, G. (2021). Metal-organic frameworks for pesticidal persistent organic pollutants detection and adsorption – a mini review. *J. Hazard. Mater.* 413, 125325. doi:10.1016/j.jhazmat.2021.125325
- Wang, D., Jia, F., Wang, H., Chen, F., Fang, Y., Dong, W., et al. (2018). Simultaneously efficient adsorption and photocatalytic degradation of tetracycline by Fe-based MOFs. *J. Colloid Interface Sci.* 519, 273–284. doi:10.1016/j.jcis.2018.02.067
- Wang, M., Mei, Y., Chen, S., Komarneni, S., and Ma, J. (2022). Porous N-doped carbon nanospheres with encapsulated cobalt nanocrystals for persulfate activation to degrade tetracycline. *Ceram. Int.* 48, 27622–27630. doi:10.1016/j.ceramint.2022.06.058
- Wang, W., Li, X., Deng, F., Liu, J., Gao, X., Huang, J., et al. (2022). Novel organic/inorganic PDI-Urea/BiOBr S-scheme heterojunction for improved photocatalytic antibiotic degradation and H₂O₂ production. *Chin. Chem. Lett.* 33, 5200–5207. doi:10.1016/j.ccl.2022.01.058
- Wang, Y., Long, Y., Yang, Z., and Zhang, D. (2018). A novel ion-exchange strategy for the fabrication of high strong BiOI/BiOBr heterostructure film coated metal wire mesh with tunable visible-light-driven photocatalytic reactivity. *J. Hazard. Mater.* 351, 11–19. doi:10.1016/j.jhazmat.2018.02.027
- Warner, A. J., Hathaway-Schrader, J. D., Lubker, R., Davies, C., and Novince, C. M. (2022). Tetracyclines and bone: Unclear actions with potentially lasting effects. *Bone* 159, 116377. doi:10.1016/j.bone.2022.116377
- Xu, G., Du, M., Li, T., Guan, Y., and Guo, C. (2021). Facile synthesis of magnetically retrievable Fe₃O₄/BiVO₄/CdS heterojunction composite for enhanced photocatalytic degradation of tetracycline under visible light. *Sep. Purif. Technol.* 275, 119157. doi:10.1016/j.seppur.2021.119157
- Yang, G., Zhu, Y.-A., Liang, Y., Yang, J., Wang, K., Zeng, Z., et al. (2021). Crystal defect-mediated {010} facets of Bi₂MoO₆ nanosheets for removal of TC: Enhanced mechanism and degradation pathway. *Appl. Surf. Sci.* 539, 148038. doi:10.1016/j.apsusc.2020.148038
- Yin, C., Liu, Y., Lv, X., Lv, S., Cheng, H., Kang, X., et al. (2022). Carbon dots as heterojunction transport mediators effectively enhance BiOI/g-C₃N₄ synergistic persulfate degradation of antibiotics. *Appl. Surf. Sci.* 601, 154249. doi:10.1016/j.apsusc.2022.154249
- Zhang, H., Wang, C., Zhang, X., Zhang, R., and Ding, L. (2020). Formation and inhibition of polycyclic aromatic hydrocarbons from the gasification of cyanobacterial biomass in supercritical water. *Chemosphere* 253, 126777. doi:10.1016/j.chemosphere.2020.126777
- Zhang, X., Xu, B., Wang, S., Li, X., Wang, C., Xu, Y., et al. (2022). Carbon nitride nanotubes anchored with high-density CuN_x sites for efficient degradation of antibiotic contaminants under photo-Fenton process: Performance and mechanism. *Appl. Catal. B Environ.* 306, 121119. doi:10.1016/j.apcatb.2022.121119
- Zhou, Z., Li, Y., Li, M., Li, Y., and Zhan, S. (2020). Efficient removal for multiple pollutants via Ag₂O/BiOBr heterojunction: A promoted photocatalytic process by valid electron transfer pathway. *Chin. Chem. Lett.* 31, 2698–2704. doi:10.1016/j.ccl.2020.07.003
- Zhu, J.-y., Li, Y.-p., Wang, X.-j., Zhao, J., Wu, Y.-s., and Li, F.-t. (2019). Simultaneous phosphorylation and Bi modification of BiOBr for promoting photocatalytic CO₂ reduction. *ACS Sustain. Chem. Eng.* 7, 14953–14961. doi:10.1021/acssuschemeng.9b03196
- Zhu, X.-D., Wang, Y.-J., Sun, R.-J., and Zhou, D.-M. (2013). Photocatalytic degradation of tetracycline in aqueous solution by nanosized TiO₂. *Chemosphere* 92, 925–932. doi:10.1016/j.chemosphere.2013.02.066